An Adaptive Identification of Rotor Time Constant for Speed-Sensorless Induction Motor Drives: A Case Study for Six-Phase Induction Machine

Mohammad Hosein Holakooie and Grzegorz Iwanski, *Senior Member, IEEE*

***Abstract*— Accurate rotor time constant (T_r) value is necessary to ensure an acceptable performance of the indirect field-oriented control (IFOC) strategy, where a detuned T_r affects rotor flux orientation and, in turn, results in poor dynamic and steady-state response of torque. The problems associated with detuned T_r will be exacerbated in sensorless drives when a model-based speed estimation algorithm is employed. This article investigates the problem of simultaneous identification of the rotor time constant and rotor speed for sensorless IFOC of six-phase induction motor (6PIM) drives. First, an adaptive observer is proposed for online detection of the low-frequency sinusoidal signal, which is intentionally injected into the rotor flux command. Then, a novel model reference adaptive system (MRAS)-based T_r estimator is proposed using the detected signal. The Lyapunov stability theorem is used to ensure the asymptotic stability of the proposed identification system. The proposed method is based on the induction machine (IM) model in primary subspace, i.e., α–β subspace. Hence, it is usable for other multiphase IM (three phases and higher). Nevertheless, the 6PIM is adopted here as a case study. The simulation and experimental results clarify the effectiveness of the proposed parallel estimation system.**

***Index Terms*— Adaptive observer, indirect field-oriented control (IFOC), model reference adaptive system (MRAS), rotor time constant estimation, sensorless, six-phase induction motor (6PIM).**

I. Introduction

ONLINE updating of the rotor time constant (T_r) is of paramount importance in the indirect field-oriented control (IFOC) strategy of induction machines (IMs). Any mismatch between the real and tuned values of the rotor time constant leads to a degraded performance of the IFOC strategy. A detuned value of the rotor time constant causes erroneous slip position calculation, which in turn leads to inaccurate rotor flux orientation [1]. The rotor time constant depends on the rotor resistance (R_r) and the rotor inductance (L_r), which may be changed by temperature drift and magnetic nonlinearity, respectively. While the rotor inductance value can be updated according to a predefined magnetizing curve of the IM [2], the problem of online updating of the rotor resistance has become a major concern [3].

A few years after the FOC strategy was proposed, research on estimating T_r and R_r began [4], [5]. A number of research works have been devoted to using the transient response of IM's characteristics to detect T_r and R_r. To address this, the rotor speed transient response has been implemented to estimate R_r in [6]. In [7], the slip gain (the inverse of T_r) has been identified during stator voltage transients caused by changing the torque command. Such techniques do not widely cover industrial applications because they can only operate during the transient period of IM. Numerous endeavors have been proposed to achieve more reliable T_r and R_r identification systems using the IM model and adaptive control techniques. The model reference adaptive system (MRAS) technique-based T_r estimator [3], [8], [9] and R_r estimator [10], [11] have been frequently discussed. The rotor time constant and rotor resistance identification systems based on adaptive full-order observers have been presented in [12]–[15], where advancing the development of an accurate and stable estimator is the main goal. Extended Kalman filter (EKF)-based R_r estimator [16], sliding-mode observer-based R_r and T_r estimators [17], and fuzzy logic and neutral network (NN)-based R_r estimator [18] are some other attempts that have been made to online update R_r and T_r using the IM model.

The advantages of speed-sensorless electric drive systems, such as lower hardware complexity and higher reliability, have been interesting enough to merit further attention in industrial applications [19]–[22]. While most of the literature addresses T_r estimation in an electric drive system equipped with a shaft encoder, providing a parallel estimation system for rotor parameters, including the rotor speed (ω_r) and T_r, remains a challenging task due to problems of the persistent excitation (PE) condition [14], [23] and simultaneous observability of T_r and ω_r in the steady-state (SS) condition [6]. Indeed, simultaneous estimation of the rotor time constant in a sensorless drive system can be possible if the rotor flux varies with time [8]. To cope with the problem of simultaneous estimation, some specific techniques have been so far introduced in the technical literature. The possibility of using transient states without signal injection for estimating T_r has been demonstrated in [6], and a new representation of

Manuscript received June 27, 2020; revised August 24, 2020 and October 12, 2020; accepted November 24, 2020. Date of publication December 3, 2020; date of current version October 1, 2021. This work was supported by the Polish National Agency for Academic Exchange through the Ulam Programme under Grant PPN/ULM/2019/1/00211/U/00001. Recommended for publication by Associate Editor Luca Zarri. *(Corresponding author: Mohammad Hosein Holakooie.)*

The authors are with the Institute of Control and Industrial Electronics, Warsaw University of Technology, 00-662 Warsaw, Poland (e-mail: hosein.holakooie@ee.pw.edu.pl; iwanskig@isep.pw.edu.pl).

Color versions of one or more figures in this article are available at https://doi.org/10.1109/JESTPE.2020.3042305.

Digital Object Identifier 10.1109/JESTPE.2020.3042305

the IM model with an adaptive observer has been showcased in [24]. EKF includes the possibility of parallel estimation of all IM's parameters due to enough excitation [16], [25]. However, it is overshadowed by computational complexity. A detuned MRAS speed estimator has been reported in [8], which has considered small-signal dynamics as a possible source of information for solving the simultaneous estimation problem. However, the conventional MRAS-based estimation system suffers from poor performance in the low-speed region (0–2.5 Hz). Detecting the rotor speed using stator circuit harmonic spectrum, caused by rotor slot openings, can rid the T_r estimation system of the simultaneous observability problem [26], [27], but this choice does not offer an appropriate dynamic performance over a wide speed range. Another solution is obtained by harmonic injection in order to continuously keep the drive system in the quasi-SS condition [15], [28]–[30]. Using the injected signal into the flux-producing current command [15], [28] or the flux command [29], [30], it is possible to provide a parallel estimation system of ω_r and T_r, which offers satisfactory performance over a wide speed range. In contrast, injecting an additional frequency component to the current or flux can yield SS torque and speed ripples [27].

Due to economic reasons and proven technologies, three-phase machines are the main choice of the market in the most adjustable-speed drives (ASDs) [31]. However, a general overview of the recent research efforts indicates that the multiphase machine-based ASDs have been extraordinarily joining the mainstream of research studies because of their interesting features [32]. The inherent fault-tolerant capability of multiphase systems is enough to attract a lot of interest for safety-critical applications, such as electric vehicles, aircrafts, and ships [33]. The reason behind this interesting feature is the stator phase redundancy, which provides the higher number of degrees of freedom in comparison with three-phase counterpart. The phase redundancy offers extra merits, such as higher reliability, lower rate of power switches, and lower torque pulsations [34]. Among different structure of multiphase IMs, five- and six-phase IMs are more interested, due to compromise between complexity and potential benefits, where the six-phase induction motor (6PIM) is the beneficiary of the three-phase technology because of its modular structure [35]. In this article, a 6PIM is adopted as a case example to validate the effectiveness of the proposed technique. Nevertheless, the proposed strategy can be implemented for other IM drives with an arbitrary number of phases (three phases and higher).

Aiming to overcome some shortcomings of the current parallel estimation systems of T_r and ω_r, including poor dynamic performance of the speed estimator [27], high computational burden [16], poor performance of the estimation in the SS condition at low speeds [8], inability of estimation under speed and load changes [29], and lack of generality [6], this article proposes a novel MRAS-based T_r estimation system. Among these identification methods, the proposed scheme in addition to [29] is based on injection of a low-frequency signal to the rotor flux command. This article employs an amplitude-adaptive state observer to separately estimate the amplitude of the injected signals using voltage and current models, whereas Wang *et al.* [29] provided the rotor time constant using the ratio of the injected amplitudes with some simplified assumptions. The amplitude estimation process gives the possibility of using the valid MRAS technique to estimate T_r, which in turn offers some benefits such as better convergence rate and estimation ability under speed and load transients.

In this article, the simultaneous estimation problem of the rotor time constant and the rotor speed in 6PIM drives is investigated by a novel solution based on an adaptive observer for estimating the amplitude of a sinusoidal signal, which is intentionally injected into the rotor flux command. Regarding the impossibility of simultaneous estimation of T_r and ω_r using classical MRAS schemes, the rotor flux is perturbed by a small low-frequency ac signal, where its low amplitude alleviates significant torque ripples in the SS condition, and its low frequency avoids the need for high-grade transducers as well as fast analog-to-digital converters (ADCs). This procedure is common among signal injection-based schemes [29], [30]; however, the extraction method of T_r after signal injection is the novelty of this article, and to the best of the author's knowledge, there is no such an MRAS technique for neither the three-phase nor the multiphase (more than three) IMs. The main goals of the proposed algorithm are to decouple the rotor time constant and the speed estimation systems as well as to satisfy the PE condition while maintaining the acceptable SS performance of the drive system. The proposed T_r estimator is incorporated into a sensorless electric drive system based on the rotor flux-based MRAS strategy for obtaining the rotor speed. Specifically, this article presents the following contributions.

1) An amplitude-adaptive state observer with a new formulation is proposed to detect the amplitude of the injected signal. The stability of the observer is discussed using the Lyapunov stability theorem.
2) A novel MRAS technique is proposed using the voltage and current models of the 6PIM as well as the aforementioned amplitude-adaptive observer, where its asymptotical stability is ensured using the Lyapunov stability method.
3) The proposed T_r estimation system is experimentally validated in a sensorless IFOC drive system based on the 6PIM as a case example.

II. Background of the Sensorless 6PIM Drive System

A. Topology of Converter-Fed 6PIM

The topology of the adopted asymmetrical 6PIM supplied from two voltage source converters (VSCs) is shown in Fig. 1. The asymmetrical 6PIM is obtained by two sets of three-phase winding spatially displaced by 30°e. Availability of the two isolated neutral points can provide optimized dc-link utilization and avoid zero-sequence currents. The modular structure of the 6PIM offers the possibility of using modular VSCs.

Using the vector space decomposition (VSD) approach [36], the constructed phase voltages can be transferred from a normal six-phase system (a–x–b–y–c–z) into decoupled

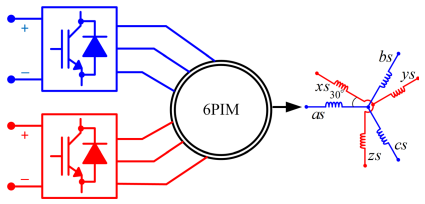

Fig. 1. Topology of asymmetrical 6PIM supplied from three-phase VSCs.

orthogonal subspaces (α–β, μ_1–μ_2, and o_1–o_2). For this purpose, the amplitude-invariant Clarke transformation matrix is used as

$$\boldsymbol{T}_6 = \frac{1}{3}\begin{bmatrix} 1 & \cos(\phi) & \cos(4\phi) & \cos(5\phi) & \cos(8\phi) & \cos(9\phi) \\ 0 & \sin(\phi) & \sin(4\phi) & \sin(5\phi) & \sin(8\phi) & \sin(9\phi) \\ 1 & \cos(5\phi) & \cos(8\phi) & \cos(\phi) & \cos(4\phi) & \cos(9\phi) \\ 0 & \sin(5\phi) & \sin(8\phi) & \sin(\phi) & \sin(4\phi) & \sin(9\phi) \\ 1 & 0 & 1 & 0 & 1 & 0 \\ 0 & 1 & 0 & 1 & 0 & 1 \end{bmatrix} \tag{1}$$

where $\phi = \pi/6$. In this way, the fundamental components and the harmonics of order $12m \pm 1$, $(m = 1, 2, 3, \ldots)$ are mapped into the α–β subspace. The harmonics of order $6n \pm 1$, $(n = 1, 3, 5, \ldots)$ are mapped into the μ_1–μ_2 subspace and the zero-sequence harmonics are transferred into the o_1–o_2 subspace.

B. Mathematical Model of 6PIM

The voltage equations of the 6PIM in the stationary α–β and μ_1–μ_2 reference frames are written as follows:

$$\begin{cases} \upsilon_{s\alpha} = R_s i_{s\alpha} + p\psi_{s\alpha} \\ \upsilon_{s\beta} = R_s i_{s\beta} + p\psi_{s\beta} \\ 0 = R_r i_{r\alpha} + p\psi_{r\alpha} + \omega_r \psi_{r\beta} \\ 0 = R_r i_{r\beta} + p\psi_{r\beta} - \omega_r \psi_{r\alpha} \end{cases} \tag{2}$$

$$\begin{cases} \upsilon_{s\mu 1} = R_s i_{s\mu 1} + pL_{ls} i_{s\mu 1} \\ \upsilon_{s\mu 2} = R_s i_{s\mu 2} + pL_{ls} i_{s\mu 2} \end{cases} \tag{3}$$

with the flux linkages

$$\begin{cases} \psi_{s\alpha} = L_s i_{s\alpha} + L_m i_{r\alpha} \\ \psi_{s\beta} = L_s i_{s\beta} + L_m i_{r\beta} \\ \psi_{r\alpha} = L_m i_{s\alpha} + L_r i_{r\alpha} \\ \psi_{r\beta} = L_m i_{s\beta} + L_r i_{r\beta} \end{cases} \tag{4}$$

and the electromagnetic torque

$$T_e = 3P(\psi_{s\alpha} i_{s\beta} - \psi_{s\beta} i_{s\alpha}) \tag{5}$$

where υ, i, ψ, T, R, and L illustrate voltage, current, flux linkage, torque, resistance, and inductance, respectively. Subscripts s, r, l, and m indicate stator quantities, rotor quantities, leakage inductance, and magnetizing inductance, respectively. P and p denote pole pairs and the derivative operator, respectively. It is worth pointing out that the 6PIM model in the o_1–o_2 subspace has the same form of the μ_1–μ_2 subspace. However, the studied 6PIM has two isolated neutral points, which avoids zero-sequence currents.

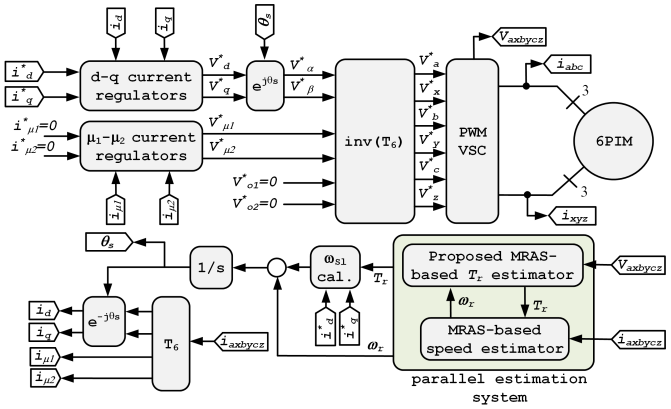

Fig. 2. Block diagram of the sensorless IFOC scheme.

C. Rotor Flux-Based MRAS Speed Estimation System

In this article, the rotor flux MRAS-based speed estimator is adopted to online update the rotor speed. The MRAS contains two different models, namely, the voltage and current models, which independently provide the α-axis and β-axis rotor fluxes [20]. An adaptation law is designed based on nonlinear stability theorems, such as the well-known Popov's stability method whereby the error equations of the estimated rotor fluxes must fulfill Popov's integral inequality. Accordingly, the adaptation law is deduced as (6) like in [37]

$$\hat{\omega}_r = \left(K_p + \frac{K_i}{s}\right)\epsilon_\omega \tag{6}$$

where K_p and K_i are the proportional and integral gains, respectively, and ϵ_ω is the speed tuning signal as [37]

$$\epsilon_\omega = \hat{\psi}_{r\alpha C}\hat{\psi}_{r\beta V} - \hat{\psi}_{r\beta C}\hat{\psi}_{r\alpha V} \tag{7}$$

where subscripts V and C denote voltage and current models, respectively, which will be described in more detail later.

D. Sensorless IFOC of 6PIM

The block diagram of the sensorless IFOC strategy for the 6PIM drive system is presented in Fig. 2. A conventional current control strategy is provided by regulating the d–q synchronous reference frame currents using proportional–integral (PI) regulators. Similarly, the PI regulators are implemented for control of μ_1–μ_2 current components, where the μ_1–μ_2 current commands are set to zero for decreasing stator copper losses. Because of two isolated neutral points topology for 6PIM, the o_1–o_2 current controllers can be neglected by considering $\upsilon^*_{o1} = \upsilon^*_{o2} = 0$. In this scheme, the rotor speed is estimated by the MRAS technique and the rotor time constant is obtained by the proposed algorithm based on the adaptive observer, which will be discussed in Section III in detail. The parallel estimation system provides T_r and ω_r, simultaneously, to ensure correct field orientation. The estimated speed is also used in the outer speed control loop, which is not shown in this figure.

III. Proposed Adaptive Observer-Based Rotor Time Constant Estimator

A. Preliminary Considerations

Starting from (2) and (4), after some manipulations, the rotor flux can be calculated by the voltage model of the 6PIM as

$$\begin{cases} \hat{\psi}_{r\alpha V} = \dfrac{L_r}{L_m}(\hat{\psi}_{s\alpha} - \sigma L_s i_{s\alpha}) \\ \hat{\psi}_{r\beta V} = \dfrac{L_r}{L_m}(\hat{\psi}_{s\beta} - \sigma L_s i_{s\beta}) \end{cases} \tag{8}$$

and by the current model of the 6PIM as

$$\begin{cases} p\hat{\psi}_{r\alpha C} = \dfrac{L_m}{T_r} i_{s\alpha} - \dfrac{1}{T_r}\hat{\psi}_{r\alpha C} - \hat{\omega}_r \hat{\psi}_{r\beta C} \\ p\hat{\psi}_{r\beta C} = \dfrac{L_m}{T_r} i_{s\beta} - \dfrac{1}{T_r}\hat{\psi}_{r\beta C} + \hat{\omega}_r \hat{\psi}_{r\alpha C} \end{cases} \tag{9}$$

where $\sigma = 1 - L_m^2/L_s L_r$ is the leakage coefficient. Obviously, the rotor flux provided by the voltage model is independent of the rotor time constant, whereas for the one in the current model, this dependence exists. Based on the well-established rotor flux IFOC strategy, expressing the current model in the d–q synchronous reference frame aligned with the rotor flux, where $\psi_{rq} = 0$, yields

$$p\hat{\psi}_r = \frac{L_m}{T_r} i_{sd} - \frac{1}{T_r}\hat{\psi}_r \tag{10}$$

where $\hat{\psi}_{rd}$ is denoted by $\hat{\psi}_r$. With respect to (10), it is seen that T_r cannot be obtained by the rotor flux and the stator current information when the 6PIM is operated in the SS conditions because

$$\frac{L_m}{T_r} i_{sd} - \frac{1}{T_r}\hat{\psi}_r = 0 \Rightarrow \hat{\psi}_r = L_m i_{sd}. \tag{11}$$

This is the reason behind the injection of the time-varying component to the rotor flux command for continuously keeping the excitation of the drive system. Thus, the command value of the rotor flux is considered to be

$$\psi_r^* = |\bar{\psi}_r|^* + \Delta\psi_r^* \tag{12}$$

in which the low-frequency component is expressed by

$$\Delta\psi_r^* = A_i^* \sin\, \omega_i^* t \tag{13}$$

where A_i^* and ω_i^* are the amplitude and frequency of the injected signal, respectively. Superimposing the introduced sinusoidal perturbation $\Delta\psi_r^*$ on the rotor flux command causes harmonic components with the same frequency in the voltage and current model-based estimated rotor flux as well as the stator current. Due to (2) and (8), the harmonic component of the rotor flux obtained by the voltage model can be described as follows:

$$\Delta\hat{\psi}_{rV} = A_V \sin\big(\omega_i^* t + \phi_V\big). \tag{14}$$

Similarly, the superimposed sinusoidal component of the rotor flux by the current model (10) can be obtained in the following way:

$$\Delta\hat{\psi}_{rC} = A_C \sin\big(\omega_i^* t + \phi_C\big). \tag{15}$$

Regarding (14) and (15), some points are highlighted as follows.

1) The amplitude A_V is a function of L_r, L_s, L_m, and R_s, and the amplitude of the stator flux and current harmonics due to the injected perturbation signal. These parameters are supposed to be constant (L_r, L_s, and L_m), measurable (voltage and current harmonics), and identifiable (R_s). Hence, the modulus of the estimated rotor flux by the voltage model can be assumed as a reference parameter in the T_r estimation system.
2) The amplitude A_C is a function of L_m, T_r, ω_i^*, and the amplitude of the d-axis current harmonic A_d is due to injected perturbation signal. A_C can be calculated as
$$A_C = \frac{L_m A_d}{\sqrt{\omega_i^{*2} T_r^2 + 1}}. \tag{16}$$
Hence, the rotor flux modulus, which is estimated by the current model, is an adjustable-T_r parameter.
3) The same analysis can be extended to the phase angles ϕ_V and ϕ_C. The phase angle ϕ_C can be written as
$$\phi_C = \phi_d - \pi/2 - \tan^{-1}\big(T_r \omega_i^*\big) \tag{17}$$
where ϕ_d denotes the phase angle of the d-axis current harmonic.

The aforementioned points are the main motivations for devising a straightforward adaptive T_r estimation algorithm. The proposed approach is based on online updating of T_r and continuously checking the amplitude of $\Delta\hat{\psi}_{rV}$ and $\Delta\hat{\psi}_{rC}$. For this purpose, the amplitude of the superimposed components is provided by the adaptive observer, which is basically inspired by the nonlinear adaptive control theory [38]–[42]. Actually, the adaptive observer is explored as an effective and possible solution to online update T_r and to overcome the problem of simultaneous estimation of T_r and ω_r. The detailed formulation and stability analysis will be introduced in the following.

It should be mentioned that the parameter estimation of periodic signals is an important task in a variety of engineering applications, where the online implementation requires computational efficiency, global stability, and fast convergence rate. For this purpose, the Fourier analysis can be conventionally employed, but it may be not a favorable technique for real-time control applications due to batch processing of data [43]. A multitude of existing solutions, such as least-square method, digital filters, and statistical analysis [40], [43], which are mainly studied in the signal processing field, only guarantee the local stability of the estimation. The adaptive observer-based parameter estimation can provide all parameters of a sinusoidal signal with the benefits of global asymptotic convergence and fast convergence rate.

B. Problem Formulation

Assuming a general form of (14) and (15) as

$$\Delta\hat{\psi}_{rx} = y = A_x \sin\big(\omega_i^* t + \phi_x\big); \quad x \in \{V, C\} \tag{18}$$

which obviously satisfies

$$\ddot{y} = -\omega_i^{*2} y \tag{19}$$

and assuming $w_1 = y$ and $w_2 = \dot{y}$ as state variables, the state-space realization can be obtained as

$$\begin{cases} \dot{w}_1 = w_2 \\ \dot{w}_2 = -\omega_i^{*2} w_1 \\ y = w_1. \end{cases} \tag{20}$$

By defining the coordinate transformation as [39]

$$\begin{cases} z_1 = w_1.w_2 \\ z_2 = 0.5 w_1^2 \end{cases} \tag{21}$$

the new state-space realization is rewritten as

$$\begin{cases} \dot{\boldsymbol{z}} = \boldsymbol{A}_0 \boldsymbol{z} + \boldsymbol{\xi}(y_f, u) \\ y_f = \boldsymbol{C}_0 \boldsymbol{z} \end{cases} \tag{22}$$

with

$$\boldsymbol{A}_0 = \begin{bmatrix} 0 & -4\omega_i^{*2} \\ 1 & 0 \end{bmatrix}, \quad \boldsymbol{C}_0 = [1 \quad 0], \quad \boldsymbol{\xi} = \begin{bmatrix} a_x \omega_i^{*2} \\ 0 \end{bmatrix}$$

where $a_x = A_x^2$. Using the state-space model in (22), the amplitude-adaptive state observer as

$$\begin{cases} \dot{\hat{\boldsymbol{z}}} = \boldsymbol{A}_0 \hat{\boldsymbol{z}} + \hat{\boldsymbol{\xi}}(y_f, u) + \boldsymbol{K}(z_1 - \hat{z}_1) \\ \hat{y}_f = \boldsymbol{C}_0 \hat{\boldsymbol{z}} \end{cases} \tag{23}$$

with constant gain matrix K, guarantees that the estimation errors asymptotically tend to zero for any initial condition.

C. Amplitude Estimation System

From (22) and (23), the state estimation errors can be described as

$$\dot{\boldsymbol{e}} = \dot{\boldsymbol{z}} - \dot{\hat{\boldsymbol{z}}} = (\boldsymbol{A}_0 - \boldsymbol{K}\boldsymbol{C}_0)\boldsymbol{e} + \Delta\boldsymbol{\xi}(y_f, u) \tag{24}$$

where

$$\Delta\boldsymbol{\xi}(y_f, u) = \Delta a_x \begin{bmatrix} \omega_i^{*2} \\ 0 \end{bmatrix}$$
$$\Delta a_x = a_x - \hat{a}_x.$$

Here, the Lyapunov's stability theory is employed to devise the amplitude adaptation law as well as to ensure the global asymptotic convergence of the observer. For this, the Lyapunov candidate function is introduced as

$$\boldsymbol{V} = \boldsymbol{e}^T \boldsymbol{e} + \frac{\Delta a_x^2}{\zeta} \tag{25}$$

where ζ is a constant positive gain. The time derivative of the Lyapunov function is given by

$$\dot{\boldsymbol{V}} = \dot{\boldsymbol{e}}^T \boldsymbol{e} + \boldsymbol{e}^T \dot{\boldsymbol{e}} + \frac{2\Delta a_x \Delta \dot{a}_x}{\zeta}. \tag{26}$$

By neglecting the variation of a_x in the observer time scale, i.e., $\dot{a}_x = 0$, and regarding (24), (26) can be written as

$$\dot{\boldsymbol{V}} = \boldsymbol{e}^T [(\boldsymbol{A}_0 - \boldsymbol{K}\boldsymbol{C}_0)^T + (\boldsymbol{A}_0 - \boldsymbol{K}\boldsymbol{C}_0)]\boldsymbol{e} + \Delta\boldsymbol{\xi}^T(y_f, u)\boldsymbol{e} + \boldsymbol{e}^T \Delta\boldsymbol{\xi}(y_f, u) - \frac{2\Delta a_x \dot{\hat{a}}_x}{\zeta}. \tag{27}$$

When the first-order time derivative of the Lyapunov function (27) is a negative definite while the Lyapunov function is a positive definite, sufficient conditions for the asymptotic stability of the observer are obtained. The first term in (27) can be designed in such a way that the eigenvalues of the $[\boldsymbol{A}_0 - \boldsymbol{K}\boldsymbol{C}_0]$ matrix are located in the left half of the complex plane. Furthermore, if the gain matrix $\boldsymbol{K}$ is properly selected, the error dynamics tend to zero with adequate speed. The Lyapunov stability condition is met if the remaining terms satisfy

$$\Delta\boldsymbol{\xi}^T(y_f, u)\boldsymbol{e} + \boldsymbol{e}^T \Delta\boldsymbol{\xi}(y_f, u) - \frac{2\Delta a_x \dot{\hat{a}}_x}{\zeta} = 0 \tag{28}$$

which yields the adaptation law of the amplitude squared

$$\dot{\hat{a}}_x = \zeta \omega_i^{*2} e_{z1} \tag{29}$$

where $e_{z1} = z_1 - \hat{z}_1$. Thus, the amplitudes of the rotor flux harmonics from voltage and current models are updated according to (29) and considering $\hat{A}_x = \sqrt{\hat{a}_x}$. A trial-and-error technique is employed to provide the proper ζ gain for amplitude estimation process.

D. Sine Wave State Observer

As described in (29), the amplitude adaptation law is based on $z_1 = w_1.w_2$ state variable, which means that the introduced adaptive observer needs the derivative of the superimposed sinusoidal waveform. This is an unfavorable feature for the adaptive observer because not only does it require more information about the system but also it may be difficult to retrieve such a noisy signal with an acceptable signal-to-noise ratio. Aiming to solve this problem, a sine wave state observer is developed according to the well-established state observer design theories.

Recall the state-space realization (20) in Section III-C, which is rewritten here as

$$\begin{cases} \dot{\boldsymbol{w}} = \boldsymbol{A}_1 \boldsymbol{w} \\ y = \boldsymbol{C}_1 \boldsymbol{w} \end{cases} \tag{30}$$

where $\dot{\boldsymbol{w}} = [\dot{w}_1 \quad \dot{w}_2]^T$, $\boldsymbol{w} = [w_1 \quad w_2]^T$, $\boldsymbol{C}_1 = [1 \quad 0]$, and

$$\boldsymbol{A}_1 = \begin{bmatrix} 0 & 1 \\ -\omega_i^{*2} & 0 \end{bmatrix}.$$

Regarding the observability matrix

$$\boldsymbol{O} = \left[\boldsymbol{C}_1^T \mid \boldsymbol{A}_1^T \boldsymbol{C}_1^T\right] \tag{31}$$

is a full-rank matrix, i.e., $\text{Rank}(\boldsymbol{O}) = 2$, the state-space model (30) is completely observable. The sine wave state observer is introduced as

$$\begin{cases} \dot{\bar{\boldsymbol{w}}} = \boldsymbol{A}_1 \bar{\boldsymbol{w}} + \boldsymbol{L}(y - \bar{y}) \\ \bar{y} = \boldsymbol{C}_1 \bar{\boldsymbol{w}} \end{cases} \tag{32}$$

where $\boldsymbol{L}$ denotes the observer feedback gain matrix. By deducing (32) from (30), the observer error equation is obtained as

$$\dot{\boldsymbol{e}} = (\boldsymbol{A}_1 - \boldsymbol{L}\boldsymbol{C}_1)\boldsymbol{e} \tag{33}$$

where $\boldsymbol{e} = \boldsymbol{w} - \bar{\boldsymbol{w}}$. It is obvious that the dynamic behavior of the errors is in relation with the eigenvalues of the $[\boldsymbol{A}_1 - \boldsymbol{L}\boldsymbol{C}_1]$ matrix. In this article, the observer gain matrix is determined to ensure that the $[\boldsymbol{A}_1 - \boldsymbol{L}\boldsymbol{C}_1]$ matrix is stable, which in turn

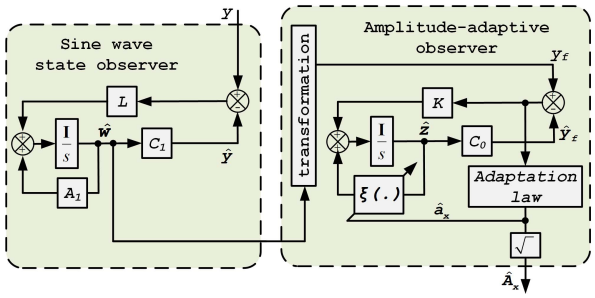

Fig. 3. Block diagram of the proposed amplitude estimation system.

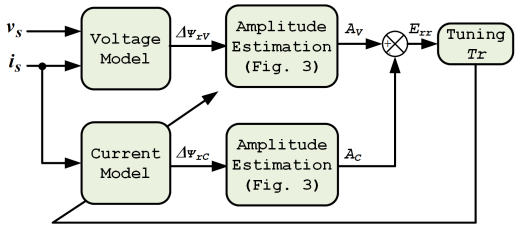

Fig. 4. Block diagram of the proposed MRAS-based T_r estimation system.

leads to a convergent sine wave state observer for any initial value of the error.

By introducing the sine wave state observer, the parameter $z_1 = w_1 w_2$ in (23) and (29) is replaced with $\bar{z}_1 = \bar{w}_1 \bar{w}_2$. The procedure for estimating the amplitude of the sinusoidal waveform is summarized in Fig. 3. It consists of the sine wave state observer and the amplitude-adaptive observer, where the first one is used to provide the new subordinate state variable $\bar{z}_1$, and the second one establishes the amplitude estimation system.

E. MRAS-Based Rotor Time Constant Estimation System

The block diagram of the proposed MRAS-based T_r estimation system is shown in Fig. 4. The superimposed low-frequency components are provided from the voltage model ($\Delta\psi_{rV}$) and the current model ($\Delta\psi_{rC}$) by subtracting the estimated rotor flux from its averaged value within a particular interval. Considering (10), it should be highlighted that the dc offset in the estimated rotor flux is not influenced by T_r. The amplitude of the superimposed components is obtained by the introduced amplitude estimation system. The value of the rotor time constant is online tuned in such a way that the error between estimated amplitudes from voltage model A_V and current model A_c is decreased. Here, an adaptation law is introduced for online updating T_r using the Lyapunov stability theorem. For this purpose, the time derivative of A_C is written as

$$\dot{A}_C = \dot{\hat{T}}_r \frac{dA_C}{d\hat{T}_r} \tag{34}$$

which regarding (16) can be simplified as

$$\dot{A}_C = -k_1 \hat{T}_r \dot{\hat{T}}_r A_C^3 \tag{35}$$

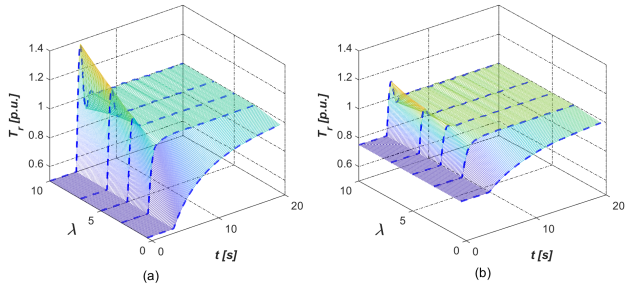

Fig. 5. Convergence of the proposed T_r estimator with different λ gains for (a) -50% and (b) -25% initial errors in T_r at 34% rated speed and rated load torque (simulation results).

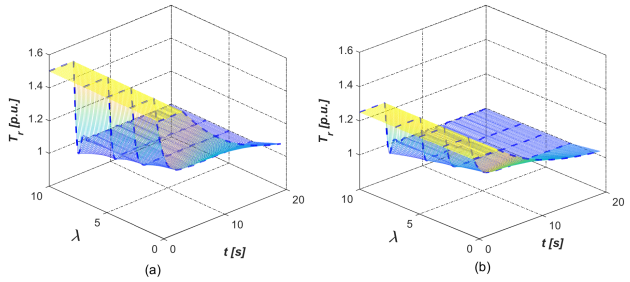

Fig. 6. Convergence of the proposed T_r estimator with different λ gains for (a) $+50\%$ and (b) $+25\%$ initial errors in T_r at 34% rated speed and rated load torque (simulation results).

where $k_1 = \omega_i^{*2}/(L_m A_d)^2$ is a positive constant. Now, the estimation error signal is presented as

$$e_T = A_V - A_C \tag{36}$$

and the error dynamics can be accordingly calculated as

$$\dot{e}_T = \dot{A}_V - \dot{A}_C = -\dot{A}_C = k_1 \hat{T}_r \dot{\hat{T}}_r A_C^3. \tag{37}$$

In (37), it is assumed $\dot{A}_V \approx 0$ because A_V is independent of the rotor time constant. Consider the following Lyapunov function candidate:

$$V_T = e_T^2 \tag{38}$$

which calculating its time derivative, with consideration of (37), yields

$$\dot{V}_T = 2e_T \dot{e}_T = 2e_T k_1 \hat{T}_r \dot{\hat{T}}_r A_C^3. \tag{39}$$

Given $\hat{T}_r > 0$, $A_C^3 > 0$, and $k_1 > 0$, an adaptation law as

$$\hat{T}_r = -\lambda \int (A_V - A_C) dt \tag{40}$$

with $\lambda > 0$, sufficiently ensures the asymptotic stability of the rotor time constant estimation system because substituting $\dot{\hat{T}}_r = -\lambda e_T$ in (39) obtains

$$\dot{V}_T = -2\lambda k_1 \hat{T}_r A_C^3 e_T^2 < 0 \tag{41}$$

which is a negative definite function.

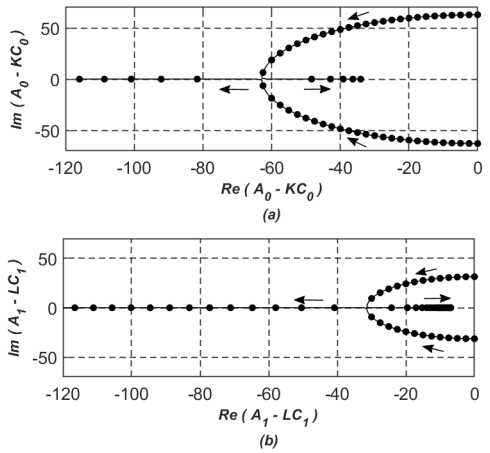

Fig. 7. Pole placement of observer for different gain values. (a) $[\boldsymbol{A}_0 - \boldsymbol{K}\boldsymbol{C}_0]$ matrix for different values of k_a. (b) $[\boldsymbol{A}_1 - \boldsymbol{L}\boldsymbol{C}_1]$ matrix for different values of l_a.

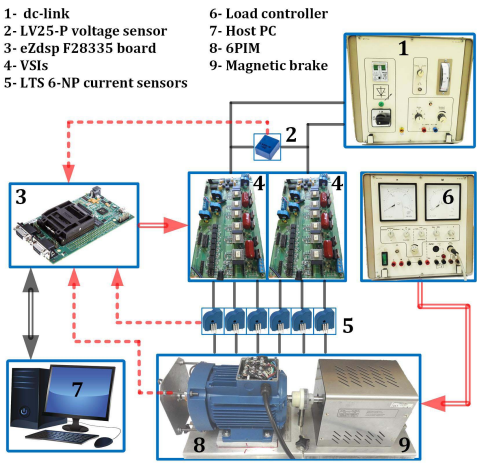

Fig. 8. Configuration of the experimental test bench.

IV. Simulation and Experimental Validation

A. Simulation Analysis

To verify the analytical discussion obtained so far, a number of simulations have been carried out using the MATLAB/Simulink environment. The selected simulation results, demonstrating convergence of the proposed T_r estimation systems for different initial errors of T_r and estimator's gains λ, are shown in Figs. 5 and 6. The underestimated and overestimated T_r take the values [0.5 0.75] and [1.25 1.5] in per unit, respectively. As can be seen, the estimated T_r is converged to the real value when it is activated at $t = 4$ s, in which its convergence rate depends on λ. A large enough value for λ increases the convergence rate and eliminates the SS error of the estimator, thus allowing the fast tracking of T_r. However, an exaggerated value, for example, $\lambda = 10$, may cause overshoot (for underestimation case) or undershoot (for overestimation case). Selection of $\lambda = 3$ ensures acceptable transient and SS performance for simulations. Such a tuning method has been employed for obtaining the appropriate value of λ in experiments.

It is worth mentioning that the gain matrices $\boldsymbol{K}$ and $\boldsymbol{L}$ are determined using pole placement in such a way that the observer poles move to the left of the system poles. For the sine wave state observer, selecting $\boldsymbol{L} = [l_a \ 0]^T$ obtains the characteristic polynomial as

$$|s\boldsymbol{I} - (\boldsymbol{A}_1 - \boldsymbol{L}\boldsymbol{C}_1)| = s^2 + l_a s + \omega_i^{*2} \tag{42}$$

where $l_a > 0$ is enough to provide a Hurwitz stable polynomial. In a similar way, selecting $\boldsymbol{K} = [k_a \ 0]^T$ provides a Hurwitz polynomial for amplitude observer. The trajectory of the observer poles for different gain values is shown in Fig. 7. As can be seen for both cases, a very large gain leads to a dominant pole close to the origin, whereas a very small gain causes complex conjugate poles close to the imaginary axis. Adopting $k_a = 4\omega_i^*$ and $l_a = 2\omega_i^*$ offers an acceptable response with fast convergence rate for amplitude and sin wave observers, respectively.

TABLE I
Parameters of 6PIM

Symbol	Quantity	Value
p	Nominal power	1 hp
P	Pole pairs	1
R_s	Stator resistance	4.08 Ω
R_r	Rotor resistance	3.73 Ω
L_s	Stator inductance	443.6 mH
L_r	Rotor inductance	443.6 mH
L_m	Magnetizing inductance	429.8 mH

B. Test Bench

The configuration of the experimental test bench is shown in Fig. 8. The test bench is based on the TMS320F28335 digital signal controller (DSC) programmed through code composer studio (CCS) development environment. The digital motor control (DMC) and IQmath libraries have been employed to provide optimized code. The switching frequency is 8 kHz with a dead band of 2 μs. The machine is fed from two three-phase converters connected to a 300-V dc power supply. The experimental results have been captured using serial communications interface (SCI) module on the eZdsp F28335 board and Advantech PCI-1716 data acquisition card and then plotted by MATLAB. An incremental encoder with 2500 pulses/revolution has been used to measure the rotor speed for validation purposes. Two IGBT-based VSIs are implemented to supply 6PIM and maintain load torque.

A 1-hp three-phase induction motor has been rewound to provide an asymmetrical 6PIM, in which its specifications are shown in Table I. It should be mentioned that, in general, the sensorless techniques may be more attractive for low-power ranges (less than 20 hp) because cost- and size-saving aspects are more important for low-power applications, while the overall cost of high-power components dominates the cost of the control system, including the transducers. Nevertheless, the proposed estimation system can be used for higher power ranges. In this regard, the sensitivity function of the estimation

error signal with respect to a detuned T_r as

$$\frac{\partial e_T}{\partial(\Delta T_r)} = -\frac{A_d L_m T_r \omega_i^{*2}}{\sqrt{\left(1+\omega_i^{*2} T_r^2\right)^3}} \tag{43}$$

shows that it is less affected by T_r changes for high-power machines due to larger T_r and smaller L_m. On the other hand, the high-power machines have better noise immunity because of higher level of the rated values.

C. Underestimation of T_r

In this test, the 6PIM is operated with an underestimated value of T_r at 34% rated speed ($\omega_r = 100$ rad/s), rated load torque ($T_L = 2$ Nm), and rated rotor flux ($\psi_r^* = 0.4$ Wb). The frequency and amplitude of the injected signal are chosen as 10% and 5% rated values, respectively, in all experiments. The validity of the proposed T_r estimator is confirmed if it replaces the detuned T_r value with its correct value when the estimation process is turned on. The initial value for T_r is set to $0.75T_r$ and $0.5T_r$. Fig. 9(a) shows the experimental results of the T_r estimation process, rotor speed error, and the superimposed rotor flux components by the voltage and current models, i.e., $\Delta\hat{\psi}_{rV}$ and $\Delta\hat{\psi}_{rC}$. When the T_r adaptation is activated at $t = 2$ s, T_r is converged to its real value. During the T_r mismatch, the superimposed component by the current model is higher than the component provided by the voltage model, in which this error vanishes immediately.

D. Overestimation of T_r

In Fig. 9(b), the sensorless drive system is executed to verify the effectiveness of the proposed T_r estimation system for overestimated values of T_r. The initial detuning in T_r takes the values of 150% and 200% of the actual value. It can be seen that overestimated T_r produces the speed error in the reverse way of the underestimated one. The error between the real and the estimated speeds as well as the error of superimposed components is removed when T_r reaches the real value using the proposed adaptation mechanism.

E. Low-Speed Operation

The low speeds together with the applied high load torque are the most critical region for many T_r identification algorithms due to multiple problems, such as instability [8], immeasurable higher order harmonics [6], and considerable error in the observed state variables [35]. For this purpose, some experiments are carried out to show the performance of the proposed T_r estimation system at the low-speed region. Fig. 10(a) reflects these results at 1.7% rated speed, 50% rated load torque, and rated rotor flux. In this case, the sensorless 6PIM drive system is run for both overestimated and underestimated T_r. It is evident that the rotor time constant is recovered after its activation at $t = 2$ s. The lower rate of convergence of the T_r estimation process is observed because of the lower level of input tuning signal. However, supposing that only the temperature-induced changes in the rotor time constant, the convergence rate seems enough because a sudden change of T_r is practically rare in normal operation. The estimated

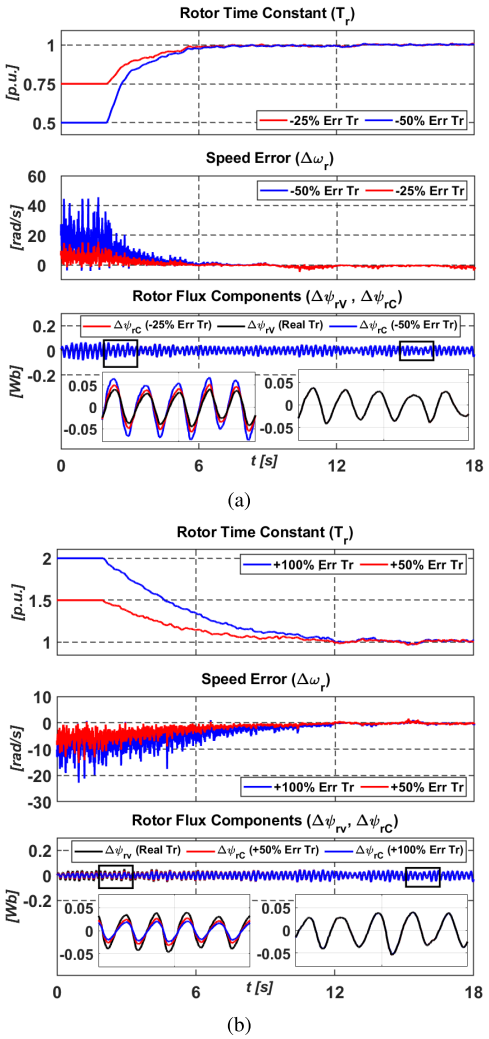

Fig. 9. Experimental results of the T_r adaptation behavior for (a) underestimated and (b) overestimated initial values at 34% rated speed and rated load torque.

amplitudes A_V and A_V of the superimposed components are also shown in Fig. 10(a), where the T_r adaptation removes the produced error between A_V and A_C.

F. No-Load Operation

In this test, the drive system is allowed to work with detuned T_r values under no-load condition at 4.8% rated speed for $\pm 50\%$ initial error in the T_r value. The results of this test are shown in Fig. 10(b). As with previous tests, the rotor time constant is accurately converged to its real value after some time. Furthermore, it can be seen that the T_r mismatch has a lower effect on the speed error under no-load condition. The produced oscillations of the speed error around the zero point are suppressed after T_r correction.

G. Speed and Load Changes

The performance of the proposed T_r estimation system under speed and load changes is investigated in this section. Fig. 11(a) shows the results of T_r adaptation behavior under

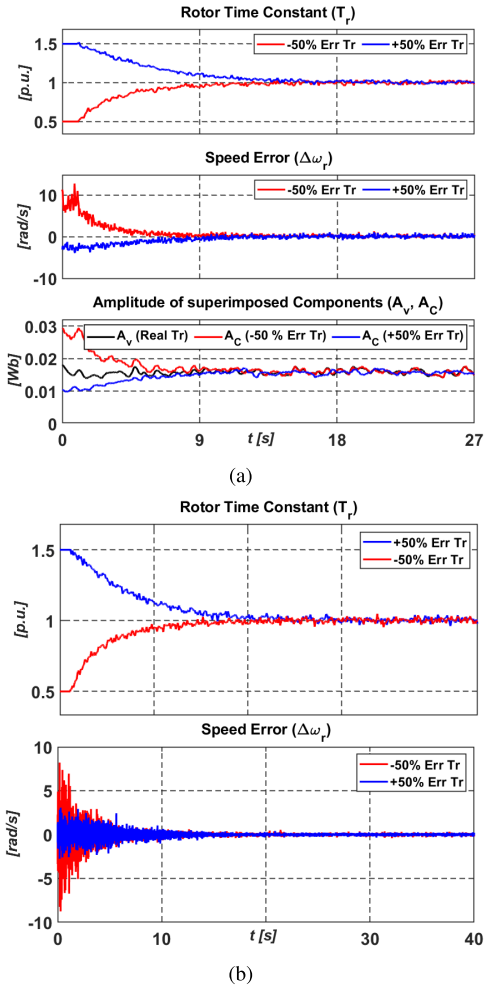

Fig. 10. Experimental results of the T_r adaptation behavior at (a) 1.7% rated speed under 50% rated load torque and (b) 4.8% rated speed under no load condition.

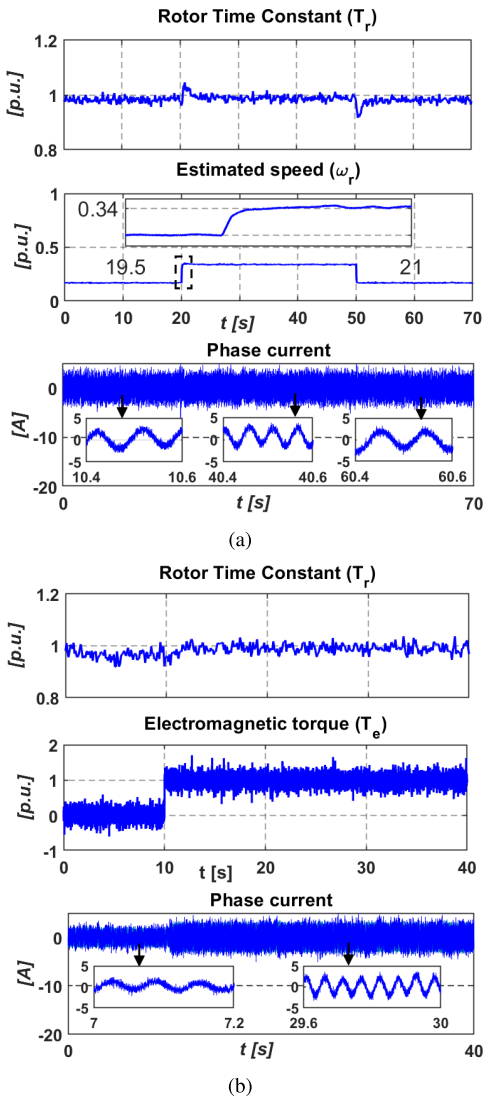

Fig. 11. Experimental results of T_r adaptation behavior for (a) speed changes from 17% to 34% rated speed and vice versa under rated load and (b) load torque change from 0% to rated load at 34% rated speed.

speed changes from 17% to 34% rated speed and vice versa at the rated load torque. The experimental results of T_r estimation process under load torque changes from 0% to rated value at 34% rated speed are shown in Fig. 11(b). The related stator current waveforms for each test scenario are also included in these figures. These scenarios reveal that the proposed estimator tracks very closely the actual T_r when sudden speed and load changes take place at SS condition. Hence, the robustness of the proposed estimator against speed and load toque disturbances can be observed. On the other hand, these results confirm that the injected low-frequency signal has a negligible impact on the SS torque response because of its low amplitude, while the speed response is less affected due to the natural filtering performed by the mechanical part. It should be highlighted that the impact of the injected signal will be intensified at very low-speed regions.

H. Stator Resistance Mismatch

The aim of this section is to demonstrate the negative effect of R_s mismatch on T_r estimation system, accordingly, importance of applying an R_s compensator to solve this problem. It should be mentioned that this problem is common among many model-based T_r estimation systems. However, it is maturely investigated in previous works; hence, there are a multitude of possible solutions to deal with it.

According to (8), the voltage model of the 6PIM is affected by the stator resistance mismatch when the value set for R_s on the controller differs from its real value on the motor. Actually, besides T_r, R_s may vary due to thermal drift impact. Inaccuracies in the stator resistance can dramatically overshadow the performance of the sensorless IFOC of the 6PIM, particularly at low speeds, where the magnitude of the induced back electromotive force (BEMF) decreases and becomes comparable with the voltage drop across R_s. The high-speed operation is marginally degraded by the R_s mismatch because the voltage drop across R_s is negligible compared to the BEMF magnitude. Fortunately, many works have been developed to tackle this problem ranging from R_s linear mapping by temperature sensor [17] and online identification of R_s [15], [35] to modified estimation of the stator flux [20].

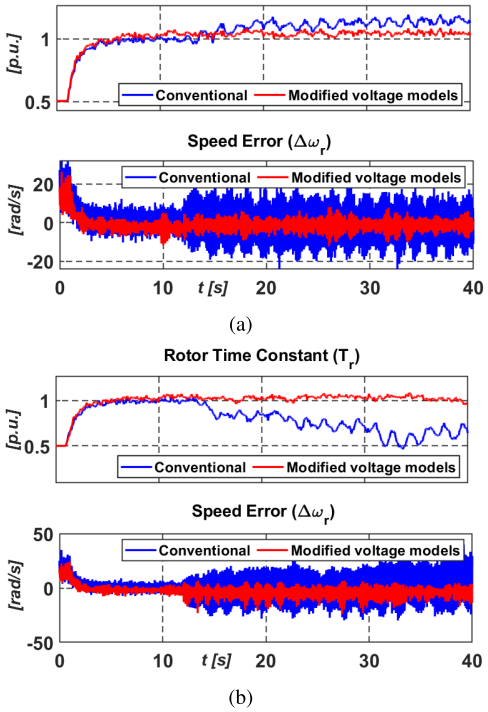

Fig. 12. Experimental results of the T_r adaptation behavior at 17% rated speed and rated load torque under (a) −30% and (b) +30% stator resistance mismatch with conventional and compensated voltage models.

This article takes R_s mismatch into account by implementing a compensated voltage model, instead of the conventional one, as described in [20], where the voltage model was modified using a supertwisting-algorithm-based second-order sliding mode (ST-SOSM) technique as follows:

$$\begin{cases} \dot{\hat{\psi}}_{s\alpha} = -R_s i_{s\alpha} + \upsilon_{s\alpha} - f(e_{i\alpha}) \\ \dot{\hat{\psi}}_{s\beta} = -R_s i_{s\beta} + \upsilon_{s\beta} - f(e_{i\beta}) \end{cases} \tag{44}$$

where $f(e_{i\alpha})$ and $f(e_{i\beta})$ are two corrective terms as a function of the current error according to the supertwisting algorithm (STA) [20], which can be generally defined as

$$f(s) = -\alpha|s|^{0.5}\text{sign}(s) - \beta \int \text{sign}(s)dt \tag{45}$$

where α and β are the constant parameters of STA. It should be emphasized here that the described ST-SOSM voltage model is one possible solution to solve the problem of R_s uncertainty, whereas the other compensation techniques, more straightforward or even sophisticated techniques, can also be implemented.

Some experiments are performed to investigate the impact of the stator resistance mismatch on the proposed T_r estimation system. Fig. 12(a) and (b) shows the behavior of the sensorless drive scheme equipped with the proposed T_r estimator at 17% rated speed and the rated load torque, under ±30% stator resistance mismatch with conventional and compensated voltage models. As expected, the conventional voltage model fails to estimate T_r correctly when the stator resistance is intentionally changed at about $t = 12$ s, which leads to speed errors and oscillations. The compensated voltage model ensures accurate T_r estimation during overestimation and underestimation of the stator resistance.

TABLE II
COMPARISON ITEMS

Item	Description
1	Independency of parameters (especially R_s)
2	Generality
3	SS adaptation ability (especially at low speeds)
4	Adaptation ability under load and speed changes
5	Simplicity
6	Fast and global convergence properties
7	Ripple-free performance in SS condition
8	Dynamic performance of the speed estimator
9	Dynamic and SS response of the torque

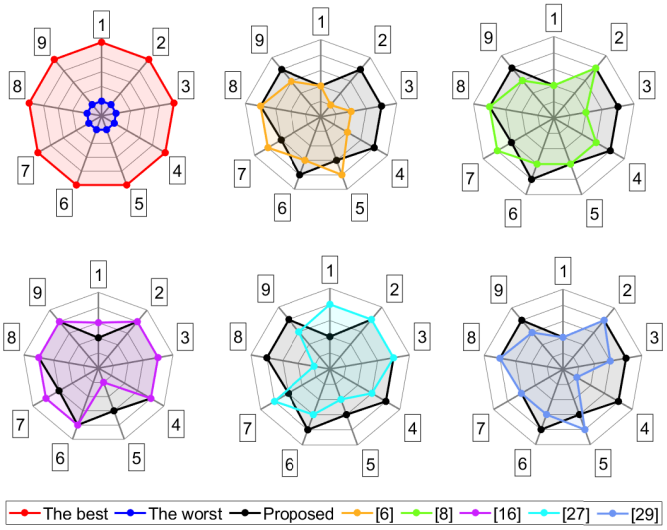

Fig. 13. Spider diagram for qualitative comparison between the proposed method and [6], [8], [16], [27], and [29].

I. Overall Analysis and Comparison

A qualitative comparison with prior arts, presented in [6], [8], [16], [27], and [29], clarifies the advantages and disadvantages of the proposed scheme. Furthermore, for some comparison indices, a quantitative comparison between the proposed method and [29], as the closest work, is reported by numerical simulations. The qualitative comparison has been performed by technical discussion and results of the aforementioned papers as well as the simulation and experimental results of this article. There are multiple indices to evaluate such a system, which are tabulated in Table II. A summary of comparison, which is also shown in Fig. 13 as a spider diagram, is as follows.

Item 1: One drawback of the proposed estimation system, besides [6], [8], [16], and [29], is the R_s dependence, which is a temperature-dependent parameter. The method presented in [27] removes this dependence using a rotor slot harmonic-based speed estimator. Hence, a supplementary technique for considering R_s variations is necessary to ensure an accurate estimation of T_r, which was discussed in Section IV-H. The EKF technique, presented in [16], inherently compensates the R_s

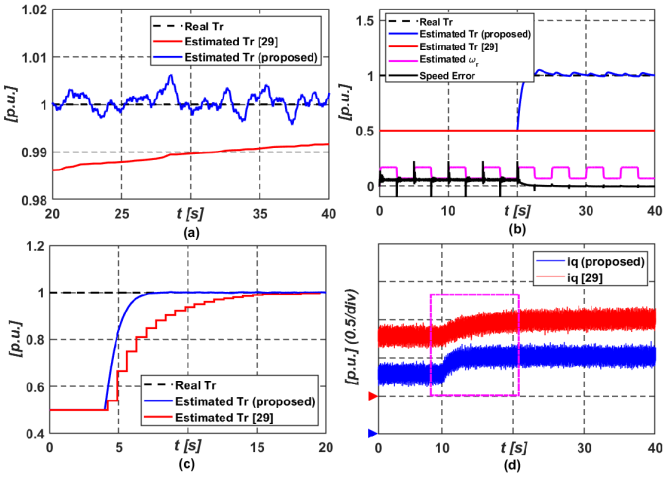

Fig. 14. Quantitative comparison of the proposed T_r estimation system and [29] using numerical simulations. (a) SS adaptation ability (item 3). (b) Adaptation ability under speed changes (item 4). (c) Fast and global convergence properties (item 6). (d) Dynamic response of the torque-producing stator current (item 9).

variations and, hence, takes a higher score against [6], [8], and [29] and the proposed scheme.

Item 2: The application range of the transient response-based T_r estimation systems (see [6]) is limited. The proposed technique, besides [8], [16], [27], and [29], can track actual T_r value at SS condition without need for transient response of motor's characteristic (see Section IV-G).

Item 3: This index considers SS adaptation ability of T_r, especially at low speeds, regardless of parameter dependence, because the latter case was discussed in item 1. As reported in [8], the method is penalized by a potential instability problem at low speeds due to the change of sign of T_r error. On the other hand, for the signal injection-based techniques, i.e., the proposed method and [29], the superimposed sinusoidal component is deteriorated by the low-frequency harmonics at low speeds. However, the proposed scheme can accurately track the distorted ac components by the amplitude-adaptive observer, whereas the method mentioned in [29] may suffer from SS estimation errors, especially at low speeds. The underlying reason is that the adaptation law of the proposed method, defined by (40), can eliminate the SS errors by the integral gain, whereas [29] considers a predefined threshold value to judge the convergence of the estimation algorithm. This issue is clarified by the comparative results shown in Fig. 14(a), where the speed command is 4.8% rated speed under rated load torque. Hence, the proposed method with [16] and [27] has better performance from this point of view (see Section IV-E).

Item 4: As discussed in [29], the method cannot follow the actual T_r when the speed command or load torque is changed largely. On the other hand, the method presented in [6] just tracks T_r value under speed transients. However, the proposed method and [8], [16], and [27] can execute under both speed and load torque changes (see Section IV-G), where the proposed method and the EKF method present a better dynamic behavior, in which this property will be more discussed in the next items. Fig. 14(b) shows the adaptation capability of the proposed T_r estimation scheme in comparison with [29] during consecutive speed changes under rated load torque.

Item 5: From simplicity viewpoint, the EKF method [16] is always criticized for its high computational burden. Real-time implementation of the particle swarm optimization (PSO)-based T_r estimation system, presented in [27], is also a challenging task for a wide range of digital processors. However, Akatsu and Kawamura [6] and Wang *et al.* [29] presented more simple techniques. The proposed method in comparison with [29] requires more computational effort because the adaptation law of [29] is more simple without need for amplitude-adaptive observer.

Item 6: The proposed method with [16] follows the actual T_r with a fast convergence rate and global stability. For the proposed technique, the fast convergence rate can be obtained by an appropriate selection of λ (see Section IV-A). However, the methods mentioned in [6], [27], and [29] may not meet the global convergence property and fast convergence rate simultaneously, for a wide range of speed. In this regard, Fig. 14(c) compares the convergence rate of the proposed technique and [29] at about 2% rated speed without load torque. Furthermore, the technique mentioned in [8] uses inherent small-signal dynamics, which always puts the drive system under the quasi-SS condition, where their relatively small amplitude reduces the convergence rate.

Item 7: Because of the superimposed sinusoidal component of the rotor flux, the low-frequency ripples appear in the torque and speed response for the proposed scheme and [29], whereas the methods presented in [6], [8], [16], and [27] are free from this type of ripples. It should be noted that the performance of the drive system is marginally affected by the injected signal due to its low amplitude.

Item 8: It is well known that the rotor slot harmonic-based speed estimators carry out the estimation process at the expense of poor dynamic performance, and hence, the method mentioned in [27] is overshadowed by poor dynamic performance of the speed estimator, whereas the MRAS speed estimator (proposed scheme and [8] and [29]) or EKF technique [16] offers a better dynamic behavior.

Item 9: This item can be considered as another interpretation of item 6 because, during T_r mismatch, the torque response is neither instantaneous nor commanded value. For this reason, the proposed technique and EKF [16] offer better performance from this point of view. In order to clarify this discussion, a comparison of the torque-producing current between the proposed method and [29] is presented in Fig. 14(d). In this test scenario, the speed command is about 2% rated speed with

rated load torque. It can be seen that the i_q value is erroneously provided during T_r mismatch so that the proposed technique recovers the real T_r faster.

In summary, the main motivation of this article is to tackle the main shortcomings of the existing parallel T_r and ω_r estimation systems. The proposed scheme, against the transient response-based techniques such as [6], can provide the accurate T_r in the SS condition, where the torque and speed have no changes. The convergence rate of the proposed technique is comparable to the EKF technique [16], while its complexity is lower. The SS adaptation ability at low speeds and the adaptation ability under load and speed changes are the other attained merits in comparison to [8] and [29], respectively. The R_s-dependence of the proposed approach can be relaxed using well-developed R_s adaptation techniques.

V. Conclusion

The main objective of this study is to provide a parallel estimation system of the rotor time constant and the rotor speed in sensorless IFOC of IM. Since the simultaneous estimation of T_r and ω_r is impossible under the SS due to constant rotor flux, a low-frequency harmonic was injected to the rotor flux to obtain additional excitation for T_r adaptation. An amplitude-adaptive observer was proposed to detect the amplitude of the injected harmonic using voltage and current models. In this way, a sine wave state observer was introduced to observe the state variables of the superimposed component. Based on the detected amplitude, a novel MRAS-based T_r estimation system was proposed. Lyapunov's stability theorem was employed to ensure the asymptotic convergence of the proposed T_r identification system. The performance of the proposed T_r estimation system was experimentally verified in a 6PIM test bench as a case example. Nevertheless, the proposed method can be used for other multiphase IMs. The merits of the proposed T_r estimator were highlighted by a qualitative comparison of the existing schemes. To alleviate the destructive effect of R_s mismatch on the proposed T_r estimator, a compensated voltage model of the 6PIM was employed, where the related experiments showed its effectiveness.

References

[1] H. A. Toliyat, E. Levi, and M. Raina, "A review of RFO induction motor parameter estimation techniques," *IEEE Trans. Energy Convers.*, vol. 18, no. 2, pp. 271–283, Jun. 2003.

[2] K. Wang, W. Yao, B. Chen, G. Shen, K. Lee, and Z. Lu, "Magnetizing curve identification for induction motors at standstill without assumption of analytical curve functions," *IEEE Trans. Ind. Electron.*, vol. 62, no. 4, pp. 2144–2155, Apr. 2015.

[3] X. Zhang, Y. Zhang, S. Yang, Z. Xie, and P. Cao, "An improved MRAS for rotor time constant updating in induction motor drives utilizing dot product of stator current and rotor flux," *IEEE Trans. Power Electron.*, vol. 34, no. 9, pp. 8905–8915, Sep. 2019.

[4] L. J. Garces, "Parameter adaption for the speed-controlled static AC drive with a squirrel-cage induction motor," *IEEE Trans. Ind. Appl.*, vol. IA-16, no. 2, pp. 173–178, Mar. 1980.

[5] T. Matsuo and T. A. Lipo, "A rotor parameter identification scheme for vector-controlled induction motor drives," *IEEE Trans. Ind. Appl.*, vol. IA-21, no. 3, pp. 624–632, May 1985.

[6] K. Akatsu and A. Kawamura, "Online rotor resistance estimation using the transient state under the speed sensorless control of induction motor," *IEEE Trans. Power Electron.*, vol. 15, no. 3, pp. 553–560, May 2000.

[7] M. W. Degner, J. M. Guerrero, and F. Briz, "Slip-gain estimation in field-orientation-controlled induction machines using the system transient response," *IEEE Trans. Ind. Appl.*, vol. 42, no. 3, pp. 702–711, May 2006.

[8] D. P. Marcetic and S. N. Vukosavic, "Speed-sensorless AC drives with the rotor time constant parameter update," *IEEE Trans. Ind. Electron.*, vol. 54, no. 5, pp. 2618–2625, Oct. 2007.

[9] P. Cao, X. Zhang, S. Yang, Z. Xie, and Y. Zhang, "Reactive-power-based MRAS for online rotor time constant estimation in induction motor drives," *IEEE Trans. Power Electron.*, vol. 33, no. 12, pp. 10835–10845, Dec. 2018.

[10] S. Maiti, C. Chakraborty, Y. Hori, and M. C. Ta, "Model reference adaptive controller-based rotor resistance and speed estimation techniques for vector controlled induction motor drive utilizing reactive power," *IEEE Trans. Ind. Electron.*, vol. 55, no. 2, pp. 594–601, Feb. 2008.

[11] S. Yang, D. Ding, X. Li, Z. Xie, X. Zhang, and L. Chang, "A decoupling estimation scheme for rotor resistance and mutual inductance in indirect vector controlled induction motor drives," *IEEE Trans. Energy Convers.*, vol. 34, no. 2, pp. 1033–1042, Jun. 2019.

[12] F. R. Salmasi, T. A. Najafabadi, and P. J. Maralani, "An adaptive flux observer with online estimation of DC-link voltage and rotor resistance for VSI-based induction motors," *IEEE Trans. Power Electron.*, vol. 25, no. 5, pp. 1310–1319, May 2010.

[13] H. Kubota, K. Matsuse, and T. Nakano, "DSP-based speed adaptive flux observer of induction motor," *IEEE Trans. Ind. Appl.*, vol. 29, no. 2, pp. 344–348, Mar. 1993.

[14] F. R. Salmasi and T. A. Najafabadi, "An adaptive observer with online rotor and stator resistance estimation for induction motors with one phase current sensor," *IEEE Trans. Energy Convers.*, vol. 26, no. 3, pp. 959–966, Sep. 2011.

[15] H. Kubota and K. Matsuse, "Speed sensorless field-oriented control of induction motor with rotor resistance adaptation," *IEEE Trans. Ind. Appl.*, vol. 30, no. 5, pp. 1219–1224, Sep. 1994.

[16] M. Barut, R. Demir, E. Zerdali, and R. Inan, "Real-time implementation of bi input-extended Kalman filter-based estimator for speed-sensorless control of induction motors," *IEEE Trans. Ind. Electron.*, vol. 59, no. 11, pp. 4197–4206, Nov. 2012.

[17] A. B. Proca and A. Keyhani, "Sliding-mode flux observer with online rotor parameter estimation for induction motors," *IEEE Trans. Ind. Electron.*, vol. 54, no. 2, pp. 716–723, Apr. 2007.

[18] B. Karanayil, M. F. Rahman, and C. Grantham, "Stator and rotor resistance observers for induction motor drive using fuzzy logic and artificial neural networks," *IEEE Trans. Energy Convers.*, vol. 20, no. 4, pp. 771–780, Dec. 2005.

[19] T. Tuovinen and M. Hinkkanen, "Adaptive full-order observer with high-frequency signal injection for synchronous reluctance motor drives," *IEEE J. Emerg. Sel. Topics Power Electron.*, vol. 2, no. 2, pp. 181–189, Jun. 2014.

[20] M. H. Holakooie, M. Ojaghi, and A. Taheri, "Modified DTC of a six-phase induction motor with a second-order sliding-mode MRAS-based speed estimator," *IEEE Trans. Power Electron.*, vol. 34, no. 1, pp. 600–611, Jan. 2019.

[21] M. Szypulski and G. Iwanski, "Sensorless state control of stand-alone doubly fed induction generator supplying nonlinear and unbalanced loads," *IEEE Trans. Energy Convers.*, vol. 31, no. 4, pp. 1530–1538, Dec. 2016.

[22] C. U. Reddy, K. K. Prabhakar, A. K. Singh, and P. Kumar, "Speed estimation technique using modified stator current error-based MRAS for direct torque controlled induction motor drives," *IEEE J. Emerg. Sel. Topics Power Electron.*, vol. 8, no. 2, pp. 1223–1235, Jun. 2020.

[23] S. Ho Jeon, K. Kyo Oh, and J. Young Choi, "Flux observer with online tuning of stator and rotor resistances for induction motors," *IEEE Trans. Ind. Electron.*, vol. 49, no. 3, pp. 653–664, Jun. 2002.

[24] J. Chen, J. Huang, and Y. Sun, "Resistances and speed estimation in sensorless induction motor drives using a model with known regressors," *IEEE Trans. Ind. Electron.*, vol. 66, no. 4, pp. 2659–2667, Apr. 2019.

[25] M. Barut, S. Bogosyan, and M. Gokasan, "Experimental evaluation of braided EKF for sensorless control of induction motors," *IEEE Trans. Ind. Electron.*, vol. 55, no. 2, pp. 620–632, Feb. 2008.

[26] Z. Gao, T. G. Habetler, R. G. Harley, and R. S. Colby, "A sensorless rotor temperature estimator for induction machines based on a current harmonic spectral estimation scheme," *IEEE Trans. Ind. Electron.*, vol. 55, no. 1, pp. 407–416, Jan. 2008.

[27] L. Zhao, J. Huang, J. Chen, and M. Ye, "A parallel speed and rotor time constant identification scheme for indirect field oriented induction motor drives," *IEEE Trans. Power Electron.*, vol. 31, no. 9, pp. 6494–6503, Sep. 2016.
[28] H. Tajima, G. Guidi, and H. Umida, "Consideration about problems and solutions of speed estimation method and parameter tuning for speed-sensorless vector control of induction motor drives," *IEEE Trans. Ind. Appl.*, vol. 38, no. 5, pp. 1282–1289, Sep. 2002.
[29] K. Wang, B. Chen, G. Shen, W. Yao, K. Lee, and Z. Lu, "Online updating of rotor time constant based on combined voltage and current mode flux observer for speed-sensorless AC drives," *IEEE Trans. Ind. Electron.*, vol. 61, no. 9, pp. 4583–4593, Sep. 2014.
[30] I.-J. Ha and S.-H. Lee, "An online identification method for both stator- and rotor resistances of induction motors without rotational transducers," *IEEE Trans. Ind. Electron.*, vol. 47, no. 4, pp. 842–853, Aug. 2000.
[31] M. J. Duran, I. Gonzalez-Prieto, N. Rios-Garcia, and F. Barrero, "A simple, fast, and robust open-phase fault detection technique for six-phase induction motor drives," *IEEE Trans. Power Electron.*, vol. 33, no. 1, pp. 547–557, Jan. 2018.
[32] E. Levi, "Multiphase electric machines for variable-speed applications," *IEEE Trans. Ind. Electron.*, vol. 55, no. 5, pp. 1893–1909, May 2008.
[33] I. Gonzalez-Prieto, M. J. Duran, M. Bermudez, F. Barrero, and C. Martin, "Assessment of virtual-voltage-based model predictive controllers in six-phase drives under open-phase faults," *IEEE J. Emerg. Sel. Topics Power Electron.*, vol. 8, no. 3, pp. 2634–2644, Sep. 2020.
[34] H. Heidari *et al.*, "A parallel estimation system of stator resistance and rotor speed for active disturbance rejection control of six-phase induction motor," *Energies*, vol. 13, no. 5, p. 1121, Mar. 2020.
[35] M. H. Holakooie, M. Ojaghi, and A. Taheri, "Direct torque control of six-phase induction motor with a novel MRAS-based stator resistance estimator," *IEEE Trans. Ind. Electron.*, vol. 65, no. 10, pp. 7685–7696, Oct. 2018.
[36] Y. Zhao and T. A. Lipo, "Space vector PWM control of dual three-phase induction machine using vector space decomposition," *IEEE Trans. Ind. Appl.*, vol. 31, no. 5, pp. 1100–1109, Sep. 1995.
[37] C. Schauder, "Adaptive speed identification for vector control of induction motors without rotational transducers," *IEEE Trans. Ind. Appl.*, vol. 28, no. 5, pp. 1054–1061, Sep. 1992.
[38] H. Márquez, *Nonlinear Control Systems: Analysis and Design*. Hoboken, NJ, USA: Wiley, 2003.
[39] M. Hou, "Amplitude and frequency estimator of a sinusoid," *IEEE Trans. Autom. Control*, vol. 50, no. 6, pp. 855–858, Jun. 2005.
[40] X. Xia, "Global frequency estimation using adaptive identifiers," *IEEE Trans. Autom. Control*, vol. 47, no. 7, pp. 1188–1193, Jul. 2002.
[41] Z. Ding, *Nonlinear and Adaptive Control Design*. Edison, NJ, USA: IET, 2013.
[42] R. Marino and P. Tomei, *Nonlinear Control Design: Geometric, Adaptive and Robust*. Upper Saddle River, NJ, USA: Prentice-Hall, 1996.
[43] M. Hou, "Parameter identification of sinusoids," *IEEE Trans. Autom. Control*, vol. 57, no. 2, pp. 467–472, Feb. 2012.

Mohammad Hosein Holakooie received the M.Sc. degree in electrical engineering from Tabriz University, Tabriz, Iran, in 2013, and the Ph.D. degree in electrical engineering from Zanjan University, Zanjan, Iran, in 2018.

He is currently a Researcher with the Institute of Control and Industrial Electronics, Warsaw University of Technology (WUT), Warsaw, Poland, the Ulam Program supported by the Polish National Agency for Academic Exchange. His current research interest includes analysis and control of multiphase drives.

Grzegorz Iwanski (Senior Member, IEEE) received the M.Sc. degree in automatic control and robotics and the Ph.D. degree in electrical engineering from the Faculty of Electrical Engineering, Warsaw University of Technology (WUT), Warsaw, Poland, in 2003 and 2005, respectively.

From January 2006 to December 2008, he was a Research Worker involved in an international project within the Sixth Framework Programme of the European Union (EU). Since 2009, he has been an Assistant Professor with the Institute of Control and Industrial Electronics, WUT, where he became an Associate Professor in 2019. From 2012 to 2013, he was with the Renewable Electrical Energy System (REES) Team, Universitat Politècnica de Catalunya (UPC), Barcelona, Spain, within the framework of the scholarship of Polish Minister of Science and Higher Education. He is a coauthor of one monograph, three book chapters, and about 70 journal articles and conference papers. He teaches courses on power electronics, drives, and power conversion systems. His research interests include variable and adjustable speed power generation systems, photovoltaic and energy storage systems, and automotive power electronics and drives.

Dr. Iwanski provided two plenary lectures on IEEE technically sponsored international conferences: Ecological Vehicles and Renewable Energies (EVER 2015) and Joint International Conference on Optimization of Electrical and Electronic Equipment and Aegean Conference on Electrical Machines and Power (OPTIM-ACEMP 2017).